Oxide phosphors for light upconversion; Yb3+ and Tm3+ co-doped Y2BaZnO5

Etchart, I; Hernandez, I; Huignard, A; Berard, M; Laroche, M; Gillin, WP; Curry, RJ; Cheetham, AK

Oxide phosphors for light upconversion; Yb^{3+} and Tm^{3+} co-doped Y_2BaZnO_5

Isabelle Etchart,[1,2] Ignacio Hernández,[3] Arnaud Huignard,[2] Mathieu Bérard,[2] Marine Laroche,[2] William P. Gillin,[3] Richard J. Curry,[4] and Anthony K. Cheetham[1,a)]
[1]*Materials Science and Metallurgy Department, University of Cambridge, Pembroke Street CB2 3QZ, United Kingdom*
[2]*Saint-Gobain Recherche, 39 quai Lucien Lefranc 93303, Aubervilliers, France*
[3]*Department of Physics, Queen Mary University of London, Mile End Road, London E1 4NS, United Kingdom*
[4]*Advanced Technology Institute, University of Surrey, Guildford, Surrey GU2 7XH, United Kingdom*

(Received 23 July 2010; accepted 16 December 2010; published online 18 March 2011)

The optical properties of Yb^{3+} and Tm^{3+} co-doped Y_2BaZnO_5, synthesized by solid-state reaction, are investigated in detail. Three main emission bands centered around 479 nm (blue), 654 nm (red), and 796 nm (near-infrared) are observed under near-infrared laser excitation via an upconversion process. Detailed studies of the upconversion properties as a function of dopant concentrations are described and upconversion efficiencies quantified precisely. Maximum efficiencies of $\sim 1.53\%$ in the 730-870 nm near-infrared emission range and of $\sim 0.09\%$ in the 420-530 nm blue range are obtained. The results of power dependence studies and concentration dependent lifetime measurements are presented. This in-depth spectroscopic study allows us, for the first time, to identify the dominant processes involved in the upconversion mechanism of Yb^{3+}, Tm^{3+} co-doped Y_2BaZnO_5 oxides. © *2011 American Institute of Physics*. [doi:10.1063/1.3549634]

I. INTRODUCTION

The upconversion luminescence properties of rare-earth doped materials for Yb^{3+}-sensitized upconversion have been the focus of much research since the development, in the nineteen eighties, of cheap and high-powered InGaAs diode lasers emitting at around 980 nm.[1–3] Most of the rare-earth upconversion work is focused on the investigation of halides[4,5] and glasses.[6–9] In particular, heavy-metal fluoride glasses have been extensively studied (e.g., ZBLAN[10]) due to their low phonon energy. They usually present poor chemical, thermal, and mechanical properties that limit their applications. The development of highly efficient and stable materials that can upconvert at room temperature with low excitation density thresholds is required. Oxide materials[11,12] are usually very stable chemically, mechanically, and thermally, and could therefore be promising hosts for light upconversion applications. Tm^{3+} is an excellent dopant candidate for upconversion under near-infrared or visible excitation because of its favorable intra-atomic 4*f* energy level structure. Its emission properties have been reported under ~ 650 nm,[13,14] 800 nm,[15,16] 980 nm,[17–19] and 1064 nm[14,20] excitations.

In the present work, we describe results obtained on a new upconversion material, namely, Y_2BaZnO_5: Yb^{3+}, Tm^{3+}. Ln_2BaZnO_5 ternary oxide hosts were first reported by Raveau *et al.* in 1982.[21,22] Since then, they have attracted attention for their interesting magnetic and optical properties. Ln_2BaMO_5 oxides (Ln = Y, Gd and M = Zn, Cu) crystallize in the orthorhombic space group Pnma. Ln ions occupy two different sevenfold coordinated sites with the same symmetry but with slightly different Ln-O distances, while the M ions exhibit an unusual distorted tetrahedral coordination. Recently, the upconversion properties of Ln_2BaZnO_5: Yb^{3+}, Er^{3+} and Ln_2BaZnO_5: Yb^{3+}, Ho^{3+} (Ln = Y, Gd) under 980 nm continuous and pulsed excitation were investigated and efficient visible emissions observed in the red and the green.[23–25] In the present work, we focus on the investigation of Yb^{3+}, Tm^{3+} co-doped Y_2BaZnO_5 materials for infrared to infrared and blue upconversion. Luminescence mechanisms are elucidated through power dependence studies and lifetime measurements on samples with different dopant concentrations. Efficiencies are also reported.

II. EXPERIMENTAL

A. Synthesis of Y_2BaZnO_5: Yb^{3+}, Tm^{3+} phosphors

$Y_{2-x-y}Yb_xTm_yBaZnO_5$ phosphors (with $0 < x \leq 0.28$ and $0 < y \leq 0.04$) were synthesized by solid-state reactions. Stoichiometric amounts of Y_2O_3 (*Alfa Aesar*, 99.99%), Yb_2O_3 (*Alfa Aesar*, 99.99%), Tm_2O_3 (*Alfa Aesar*, 99.99%), ZnO (*Fisher Scientific*, 99.5%), and $BaCO_3$ (*Fisher Scientific*, 99+%) were mixed, ground together, and sintered at 1200 °C for several days with intermediate grinding stages.

B. X-ray powder diffraction analysis

X-ray powder diffraction patterns were measured using a theta-theta diffractometer (*Bruker* D8), equipped with a Cu Kα source (generator: 40 kV and 40 mA), a scintillation detector with pulse-height analysis, and a variable knife-edge collimator for high resolution x-ray diffractometry. The best achievable instrumental resolution was 0.08° in 2θ.

C. Upconversion luminescence spectroscopy

The luminescence measurements under near-infrared excitation presented in this paper were performed under either 974 or 977 nm excitation, depending on the equipment used.

a)Author to whom correspondence should be addressed. Electronic mail: akc30@cam.ac.uk.

The emission properties are the same whichever excitation wavelength is used. For emission spectra acquisition and upconversion efficiency measurements, the sample of interest was finely ground and sandwiched between two quartz plates (*Helma*, 106-QS), one of which was coated with a reflective film of silver. The sample holder was then placed at the rear face of an integrating sphere (*Instrument System*, ISP-150-100). For the acquisition of upconverted luminescence spectra, samples were excited using the 977 nm output of a temperature-controlled cw laser diode (*Thorlabs*, L980P100 and TCLDM9). The excitation signal was focused onto the center of the sample holder using a lens (*Newport*, KPX049AR.16). After initial alignment of the setup, efficiency measurements were performed in two steps. For the first measurement, the quartz sample holder at the rear-face of the integrating sphere was left empty (no sample inside, rear-face silver coated), and the laser excitation on the sample was collected using an optical fiber and analyzed with a spectrometer (*Instrument System*, CAS 140B). The incident power in the near-infrared P_{inc}^{IR} (integrated over the 950-1000 nm range) was determined from this measurement. For the second measurement, the sample under investigation was placed inside the quartz holder, and both the fraction of the excitation light that had not been absorbed by the sample (power $P_{not\ abs}^{IR}$), and the emitted upconversion light (integrated either in the 420-530 or 730-870 nm ranges) (power P_{em}^{vis}), were collected and quantified. From these two measurements, the fraction of the incident power *absorbed* by the sample was calculated. The upconversion efficiency was calculated as the ratio of the upconverted emission in the range of interest (blue: 420-530 nm or near-infrared: 730-870 nm) to the power absorbed in the 950-1000 nm range:

$$\eta_{UC} = \frac{P_{em}}{P_{abs}^{IR}} = \frac{P_{em}}{P_{inc}^{IR} - P_{not\,abs}^{IR}}.$$

A preliminary study showed that the statistical error on efficiency measurements (from repeated measurements) is on the order of 4%. The collected emissions were corrected for instrumental response.

For emission rise-time and lifetime measurements, a tunable optical parametric oscillator (OPO) (*Continuum* Panther OPO) pumped by the third harmonic wavelength at 355 nm of a Q-switched YAG: Nd laser (*Surelite* I laser) was tuned to 463 or 974 nm to excite the sample with a 7 ns pulse at a 10 Hz repetition rate. The fluorescence from the sample was separated from the pumping light using a longpass filter and was then passed through a spectrometer (*Jobin Yvon*, Triax 550) and detected using a photomultiplier tube detector (*Hamamatsu* R550) connected to a 500-MHz digital oscilloscope (*LeCroy*, 9350A) and a desktop computer.

III. RESULTS

A. Crystal structure

Figure 1 displays the typical powder x-ray diffraction pattern of Y_2BaZnO_5: Yb^{3+} (6%), Tm^{3+} (0.25%). The crystal structure is orthorhombic, space group Pnma. Relatively pure phases were obtained, as shown by the good quality of the Rietveld refinement. Cell parameters were obtained: a = 12.3358(2) Å, b = 5.7087(1) Å, and c = 7.0686(1) Å (ICDD 87082). Note that the lattice parameters are slightly smaller in the doped samples than those in the pure phases, which is attributed to the smaller ionic radii of the Yb^{3+} (0.093 nm) and Tm^{3+} (0.094 nm) compared to Y^{3+} (0.096 nm).

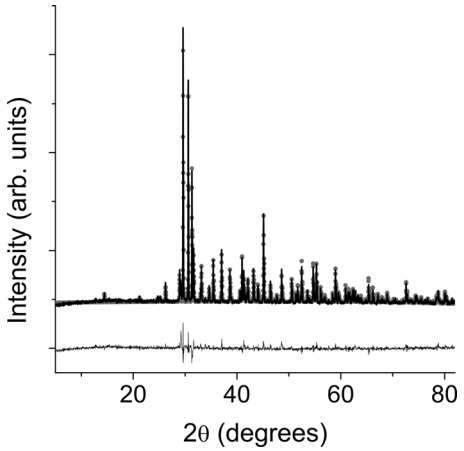

FIG. 1. Rietveld refinement based upon the x-ray powder diffraction pattern of Y_2BaZnO_5: Yb^{3+} (6%), Tm^{3+} (0.25%).

B. Upconversion luminescence emission

Following ~974 nm excitation at room temperature, Y_2BaZnO_5: Yb^{3+}, Tm^{3+} powders yield blue and red emission easily visible to the naked eye. Typical emission spectra show an intense near-infrared emission at around 796 nm, and considerably weaker visible emissions at around 479 nm (blue) and 654 nm (red) (Fig. 2). The emission spectrum measured under 463 nm excitation, corresponding to the direct excitation of the $Tm^{3+1}G_4$ state, is also presented in Fig. 2. Similar red to blue emission intensity ratios are measured under 974 and 463 nm excitation conditions. The near-infrared to blue emission intensity ratio, however, is strongly dependent on the excitation wavelength and is considerably lower under 463 nm excitation.

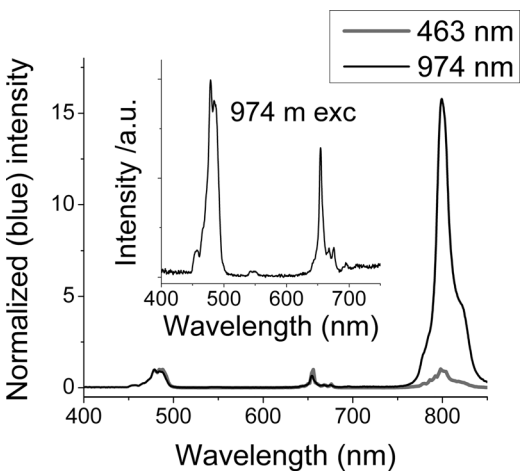

FIG. 2. Typical luminescence spectra of Y_2BaZnO_5: Yb^{3+} (6%), Tm^{3+} (0.25%) phosphors at room temperature under 974 nm excitation and 463 nm excitation. The inset presents an expansion of the emission spectra in the visible range under 974 nm excitation.

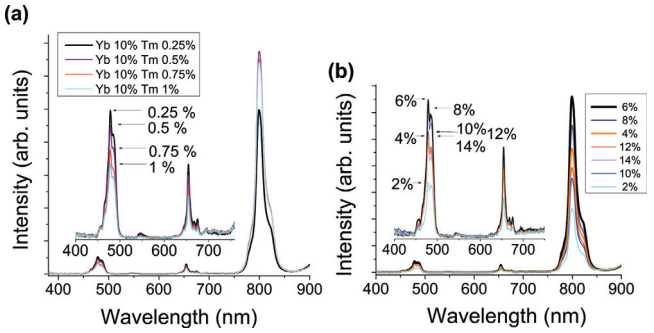

FIG. 3. (Color online) Upconversion luminescence spectra for selected samples of the: (a) Y_2BaZnO_5:Yb^{3+} (10%), Tm^{3+} (y%) (y = 0.25, 0.5, 0.75, 1.0) and (b) Y_2BaZnO_5: Yb^{3+} (x%), Tm^{3+} (0.25%) (x = 2, 4, 6, 8, 10, 12, 14) families at room temperature under ~977 nm excitation.

The down-conversion emission spectra in the infrared of Y_2BaZnO_5:Yb^{3+} (6%), Tm^{3+} (0.25%) under room temperature 974 and 463 nm excitations present broad bands centered at around 1022 and 1218 nm (Fig. S1, supplemental material[26]). Note that the 1022 nm emission is also observed under 790 nm excitations of the sample (Fig. S2, supplemental material[26]).

C. Concentration dependence of upconversion emission properties

The upconverted emission intensity and spectral properties depend on dopant concentrations. The emission spectra of selected samples of the Y_2BaZnO_5: Yb^{3+} (10%), Tm^{3+} (y %) (y = 0.25, 0.5, 0.75, 1.0), and Y_2BaZnO_5: Yb^{3+} (x%), Tm^{3+} (0.25%) (x = 2, 4, 6, 8, 10, 12, 14) families are presented in Fig. 3. For constant ytterbium concentration, and in the range of Tm^{3+} concentrations studied, 0.25% Tm^{3+} results in the strongest blue emission. [Fig. 3(a)]. For fixed Tm^{3+} concentrations of 0.25%, maximum blue emission is observed for Yb^{3+} concentrations around 6% [Fig. 3(b)].

The upconversion efficiencies of a variety of Y_2BaZnO_5: Yb^{3+} (x%), Tm^{3+} (y%) samples ($2 \leq x \leq 14$ and $0 \leq y \leq 2$) were measured at room temperature under 977 nm excitation (~2.5 W/cm^2 incident power) (Fig. 4 and supplemental material Fig. S3[26]). Samples containing around 0.25% of Tm^{3+} and 6% of Yb^{3+} were shown to exhibit the highest efficiencies for infrared to visible upconversion. Maximum upconversion efficiencies of 1.53 ± 0.07% (730-870 nm near-infrared emission range) and 0.086 ± 0.003% (420-530 nm blue emission range) were obtained with Y_2BaZnO_5: Yb^{3+} (6%), Tm^{3+} (0.25%) at room temperature under ~2.5 W/cm^2 excitation. The color coordinates associated to that composition are x = 0.1780 ± 0.0009; y = 0.1710 ± 0.0009.

D. Pump power dependence of the luminescence emission

Room temperature pump power density dependences of the blue (479 nm), red (654 nm), and near-infrared (796 nm) emissions under 977 nm excitation of Y_2BaZnO_5: Yb^{3+} (6%), Tm^{3+} (0.25%) were examined and the results are presented in a decadic log-log plot in Fig. 5. The near-infrared

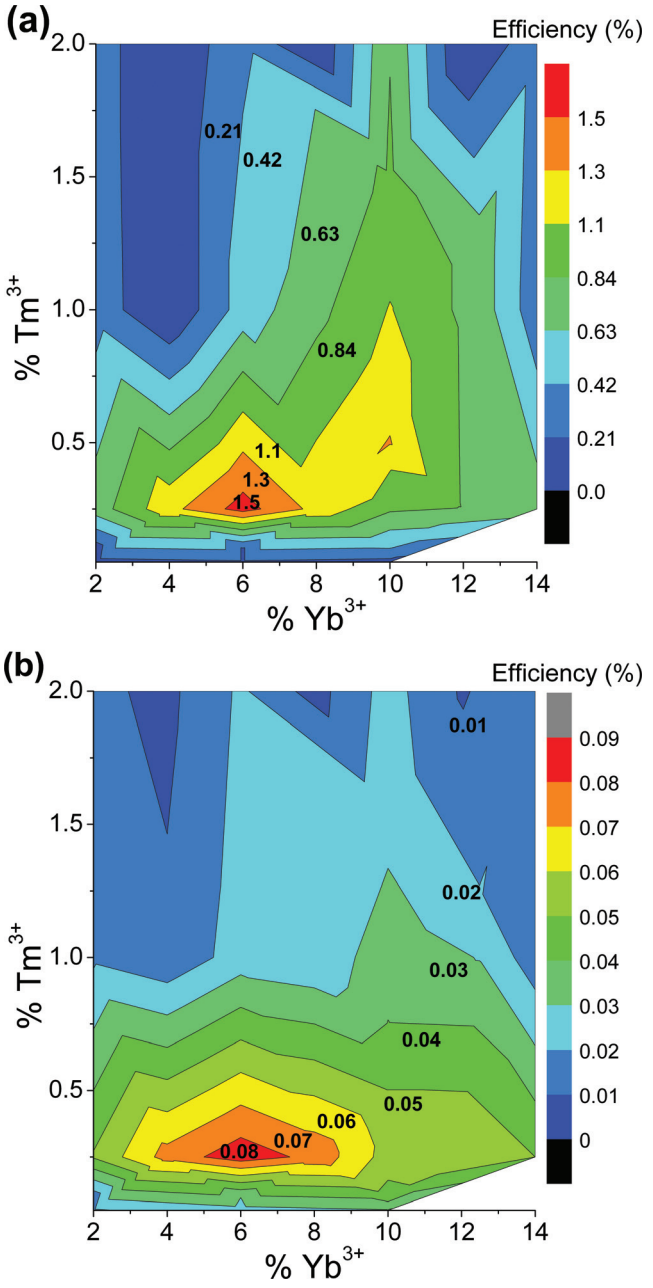

FIG. 4. (Color online) Room temperature (**a**) near-infrared upconversion efficiency in the 730-870 nm emission range and (**b**) in the 420-530 nm emission range, as a function of dopant concentration for a variety of Y_2BaZnO_5: Yb^{3+}, Tm^{3+} samples. The color bar on the right is used to display the upconversion efficiency values for each dopant composition. Contour lines (lines with the same upconversion efficiency value) and contour labels displaying the UC efficiencies associated to those contour lines are also included.

emission shows an approximately quadratic dependence on the excitation power density in the low power regime, while the blue and red emissions show a cubic behavior (Fig. 5).

E. Lifetime measurements, dopant concentration dependence

The temporal evolutions of the emissions centered at around 479, 654, 796, 1022, and 1218 nm in Y_2BaZnO_5: Yb^{3+} (6%), Tm^{3+} (0.25%) were recorded under pulsed 463 nm (direct excitation of $Tm^{3+1}G_4$) and 974 nm (excitation of $Yb^{3+2}F_{5/2}$) at room temperature. It is worth noting

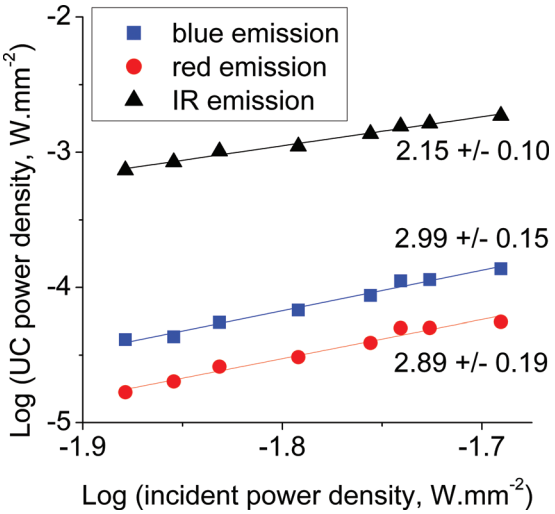

FIG. 5. (Color online) Pump power density dependence of the blue (479 nm), red (654 nm), and near-infrared (796 nm) emissions under 977 nm excitation in Y_2BaZnO_5: Yb^{3+} (6%), Tm^{3+} (0.25%) at room temperature. The results are presented in a double-decadic logarithmic scale.

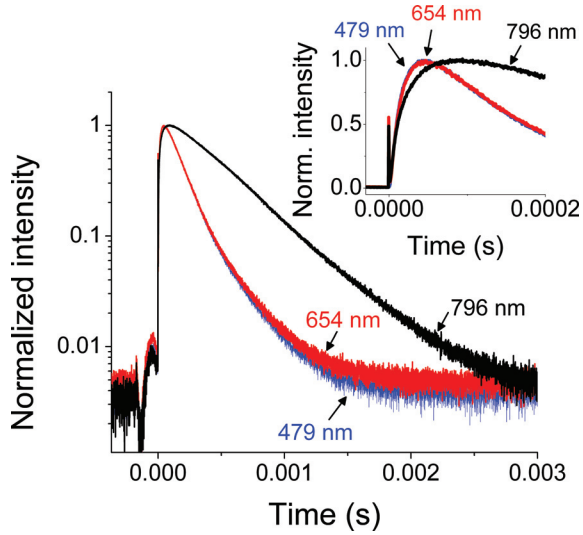

FIG. 6. (Color online) Typical temporal evolution of the blue (479 nm), red (654 nm), and near-infrared (796 nm) emissions under pulsed 974 nm excitation of Y_2BaZnO_5: Yb^{3+} (6%), Tm^{3+} (0.25%) at room temperature. The inset presents an expansion of the initial rise. Note that the small peak observed at around $t \sim -45$ μs is due to some pick-up of the radio frequency from the flashlamp firing.

that Tm^{3+} does not absorb at 974 nm, which guarantees a selective excitation of Yb^{3+} under 974 nm excitation. A typical transient corresponding to the room temperature temporal evolutions of the blue (479 nm), red (654 nm), and near-infrared (796 nm) emissions under pulsed 974 nm excitation in Y_2BaZnO_5: Yb^{3+} (6%), Tm^{3+} (0.25%) is presented in Fig. 6. At the end of the 7 ns excitation pulse, no luminescence intensity is observed; instead, the transient exhibits a typical delayed rise and a decay. This is a clear fingerprint of an energy transfer process. The experimental intensity data were fitted to the expression:[27]

$$I(t) = A\left(1 - e^{-t/\tau_r}\right)\left(e^{-t/\tau_d}\right), \tag{1}$$

where A is an emission intensity factor, and τ_r and τ_d represent the rise and decay times of the transient. Note that τ_r and τ_d are related to the transfer rate constants between Yb^{3+} and Tm^{3+} and to the intrinsic lifetimes of the states involved.[27] The decay curves showed, in some cases, a biexponential behavior, corresponding to decay mechanisms via two different depopulation channels. As such, when the transient decay section could not be fitted by a single exponential, the effective fluorescent decay time τ_d was determined using the following equation (discretization of the formula used in Ref. 28):

$$\tau_d = \frac{\sum_{i=1}^{n} A_i \tau_i^2}{\sum_{i=1}^{n} A_i \tau_i}, \tag{2}$$

where A_i and τ_i are the amplitudes and lifetimes corresponding to the depopulation channel i and $n = 1, 2$.

The room-temperature transient decay functions associated with the blue, red, and near-infrared emissions under 974 nm excitation in Y_2BaZnO_5: Yb^{3+} (x%), Tm^{3+} (y%) (x = 0, 2, 6, 10 and y = 0.25, 0.5, 1, 2) have 2, 2, and 1 distinct τ_i, corresponding to 2, 2, and 1 distinct depopulation channels, respectively. The values of the effective fluorescent decay times τ_d of the blue, red, and near-infrared emissions in these samples are listed in Table S1 (supplemental material). For instance, in Y_2BaZnO_5: Yb^{3+} (6%), Tm^{3+} (0.25%) (the composition showing the maximum upconversion efficiency that was measured in this study), the best fits associated to the blue, red, and near-infrared transients correspond to average decay times of $\tau_d = 176 \pm 9$ μs, $\tau_d = 181 \pm 9$ μs, and $\tau_d = 435 \pm 22$ μs, respectively (Fig. S4 and Table S1, supplemental material[26]). It is worth noting that the transients corresponding to the blue (479 nm) and red (654 nm) emissions have the same rise and decay times (within experimental errors) (Fig. 6).

The lifetimes associated with the room-temperature emissions around 479, 654, 796, 1022, and 1218 nm were measured for a variety of samples of the (*a*) Y_2BaZnO_5: Yb^{3+} (10%), Tm^{3+} (y%) (y = 0.25, 0.5, 1, 2) and (*b*) Y_2BaZnO_5: Yb^{3+} (x%), Tm^{3+} (0.25%) (x = 0, 2, 6, 10) families under 974 and 463 nm pulsed excitations (Fig. 7, Table S1 supplemental material). The error on lifetime measurements was estimated to be of the order 5%. For clarity, the error bars are not shown in Fig. 7(a) and 7(b).

The lifetimes associated with the blue (479 nm), red (654 nm), near-infrared (760 nm), and infrared (1022 nm) emissions under direct excitation (~463 nm) and upconversion excitation (~974 nm) decrease with increasing Tm^{3+} concentration [Fig. 7(a) and Table S1, supplemental material[26]]. The lifetimes associated with the 479 and 654 nm emissions are similar (within experimental error) in the whole range of Tm^{3+} concentrations studied. It is worth noting that, in the Tm^{3+} concentration range that we investigated, the decrease in lifetimes occurs mainly when increasing the Tm^{3+} concentration from 0.5 to 1%.

The Yb^{3+} concentration dependence of the room-temperature lifetimes associated with the 479, 654, 796, and 1022 nm emissions in Y_2BaZnO_5: Yb^{3+} (x%), Tm^{3+} (0.25%)

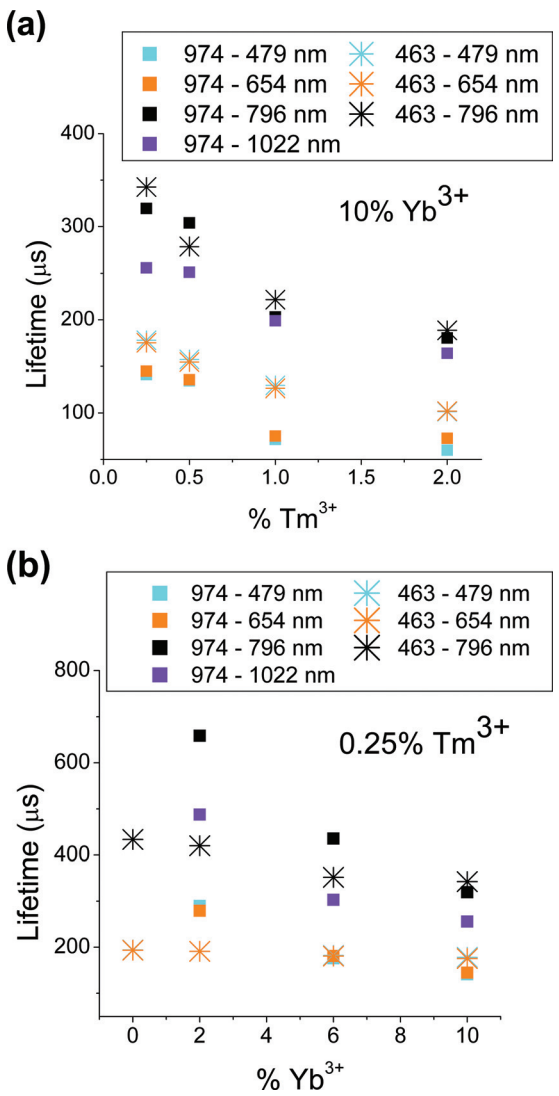

FIG. 7. (Color online) Concentration dependence of the lifetimes corresponding to the room-temperature emissions around 479, 654, 796, and 1022 nm in a variety of samples of the (a) Y_2BaZnO_5: Yb^{3+} (10%), Tm^{3+} (y%) (y = 0.25, 0.5, 1, 2) and (b) Y_2BaZnO_5: Yb^{3+} (x%), Tm^{3+} (0.25%) (x = 0, 2, 6, 10) families under 974 and 463 nm pulsed excitations. The inset shows the excitation and emission wavelengths for each set of data point.

(x = 0, 2, 6, 10) samples is shown in Fig. 7(b). The lifetimes decrease with increasing Yb^{3+} concentration. Again, the lifetimes associated with the 479 and 654 nm emissions are similar (within experimental error) in the whole range of Yb^{3+} concentrations studied (this is true under both 974 and 463 nm excitation conditions). As shown in Table S1 (supplemental material[26]), the lifetimes for all the emission centers decrease upon 974 nm excitation. The lifetimes measured under direct 463 nm excitation show a different dependence on Yb^{3+} concentration. Under 463 nm excitation, the lifetimes associated with the blue (479 nm) and red (654 nm) emissions are quasi-invariant in the Yb^{3+} concentration range that was investigated [Fig. 7(b) and Table S1, supplemental material[26]].

A careful inspection of the emission spectra in Figs. 2 and 3(a) reveals the presence of a small emission band around 454 nm. The lifetime associated with that emission is significantly shorter than that of the 479 nm emission (Fig. S5, supplemental material[26]).

IV. DISCUSSION

A. Population mechanisms of emitting states

A detailed investigation of the steady-state and dynamic emission properties of a variety of Y_2BaZnO_5: Yb^{3+} (x%), Tm^{3+} (y%) ($0 \le x \le 14$ and $0 < y \le 2$) samples was performed and the results were presented in the previous section. Under near-infrared laser excitation, the samples exhibit blue and red upconversion emissions visible to the naked eye. The emission spectra reveal the presence of emission bands centered around 479 nm (blue emission), 654 nm (red emission), and 796 nm (near-infrared emission). Under 974 nm excitation, the transients corresponding to the emissions centered at 479, 654, and 796 nm display a clear rise time after the excitation is turned off, indicating that the population mechanisms of the states from which these emissions arise involve at least one Yb^{3+} to Tm^{3+} energy transfer step (Fig. 6). Power dependence studies show that under 974 nm excitation the emission centered around 796 nm exhibits a quadratic dependence on the excitation power, indicating a two-photon population process of its emitting state(s) (Fig. 5). The emissions centered around 479 and 654 nm show a cubic dependence, indicating a three-photon population process (Fig. 5). According to the energy level diagram of Tm^{3+} represented in Fig. 8,[29] the blue emission centered at 479 nm can be exclusively assigned to the $Tm^{3+1}G_4 \rightarrow {}^3H_6$ transition. The red emission (654 nm) could be attributed to the $Tm^{3+1}G_4 \rightarrow {}^3F_4$[18,19,30] and/or $Tm^{3+3}F_{2,3} \rightarrow {}^3H_6$ transitions,[17,19,30] and the near-infrared emission (796 nm) to the $Tm^{3+3}H_4 \rightarrow {}^3H_6$[19,30,31] and/or $Tm^{3+1}G \rightarrow {}^3H_5$[18,19,30] transitions. The similarity in the lifetimes and rise-times associated with the 479 and 654 nm emissions over the whole range of concentrations studied (Figs. 6 and 7) suggests that these two emissions essentially arise from the same multiplet of Tm^{3+}, in particular ${}^1G_4$. The transient corresponding to the 796 nm emission exhibits a mono-exponential behavior (Fig. 6) with a characteristic lifetime that is significantly longer than that of the blue (479 nm) and red (654 nm) emissions (Fig. 7). In view of these results, the emissions centered at 654 and

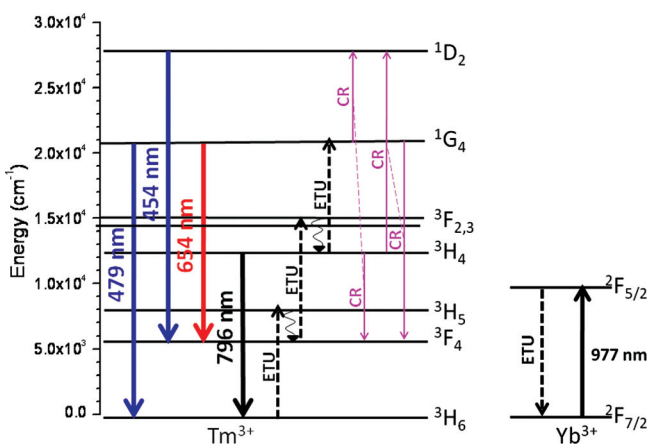

FIG. 8. (Color online) Simplified energy diagram of Tm^{3+} and Yb^{3+} ions and the dominant upconversion mechanisms in Y_2BaZnO_5: Yb^{3+}, Tm^{3+}. Blue, red, and near-infrared luminescence, as well as (nonresonant) nonradiative energy transfer upconversion (ETU), multiphonon relaxation, and cross-relaxation (CR) processes, are indicated.

796 nm can be exclusively assigned to the $Tm^{3+1}G_4 \rightarrow {}^3F_4$ and $Tm^{3+3}H_4 \rightarrow {}^3H_6$ transitions, respectively. The infrared emissions centered around 1022 nm (broad emission) and 1218 nm can be attributed to the $Yb^{3+2}F_{5/2} \rightarrow {}^2F_{7/2}$ and $Tm^{3+3}H_5 \rightarrow {}^3H_6$ transitions, respectively.

According to our findings, the population of the $Tm^{3+3}H_4$ state, from which the strong near-infrared emission at 796 nm arises, involves two successive Yb^{3+} to Tm^{3+} energy transfers with intermediate multiphonon relaxation steps; $Yb^{3+2}F_{5/2} + Tm^{3+3}H_6 \rightarrow Yb^{3+2}F_{7/2} + Tm^{3+3}H_5$ (first ET), $Tm^{3+3}H_5 \rightarrow {}^3F_4$ (multiphonon relaxation), $Yb^{3+2}F_{5/2} + Tm^{3+3}F_4 \rightarrow Yb^{3+2}F_{7/2} + Tm^{3+3}F_{2,3}$ (second ET), $Tm^{3+3}F_{2,3} \rightarrow {}^3H_4$ (multiphonon relaxation), as shown in Fig. 8. The blue (479 nm) and red (654 nm) emissions arising from the $Tm^{3+1}G_4$ state require an additional energy transfer step: $Yb^{3+2}F_{5/2} + Tm^{3+3}H_4 \rightarrow Yb^{3+2}F_{7/2} + Tm^{3+1}G_4$ (third ET).

The near-infrared (796 nm) to blue (479 nm) emission intensity ratio is much smaller under 463 nm excitation than it is under 974 nm excitation (Fig. 2). This can be assigned to the fact that, compared to the $Tm^{3+1}G_4$ state, the $Tm^{3+3}H_4$ state is relatively much more populated under upconverting conditions (by two successive Yb^{3+} to Tm^{3+} energy transfer steps) than it is by multiphonon relaxation under direct excitation of $Tm^{3+1}G_4$. Again, the population of the $Tm^{3+1}G_4$ state under upconverting conditions requires three successive Yb^{3+} to Tm^{3+} energy transfers, while the $Tm^{3+3}H_4$ state population requires only two.

B. Tm^{3+} concentration dependence of lifetimes

The decrease in $Tm^{3+1}G_4$ lifetimes with increasing Tm^{3+} concentration under direct 463 nm excitation [Fig. 7(a)] suggests the existence of cross-relaxation mechanisms between Tm^{3+} ions that depopulate the $Tm^{3+1}G_4$ state. According to the energy diagram of Tm^{3+} (Fig. 8), this could be attributed to cross-relaxations from:

1) $Tm^{3+1}G_4 + Tm^{3+3}H_4 \rightarrow Tm^{3+3}F_4 + Tm^{3+1}D_2$,[30,32]
2) $Tm^{3+3}H_4 + Tm^{3+1}G_4 \rightarrow Tm^{3+3}F_4 + Tm^{3+1}D_2$,[30,32]
3) $Tm^{3+1}G_4 + Tm^{3+3}H_6 \rightarrow Tm^{3+3}H_5 + Tm^{3+3}H_4$,[33]
4) $Tm^{3+3}H_6 + Tm^{3+1}G_4 \rightarrow Tm^{3+3}H_5 + Tm^{3+3}H_4$.[33,34]

All these processes are expected to depopulate the $Tm^{3+1}G_4$ level at high Tm^{3+} concentrations, which is in agreement with the results presented on Fig. 3(a). Processes 1) and 2) are also expected to depopulate the 796 nm emitting $Tm^{3+3}H_4$ level while processes 3) and 4) populate it. According to Fig. 3(a), for Tm^{3+} concentrations higher than 0.5%, the 796 nm emission intensity decreases with increasing Tm^{3+} concentration; processes 3) and 4) can therefore be ruled out. Careful scrutiny of the emission spectra in Fig. 2 and Fig. 3(a) reveals the presence of a small emission band around 454 nm. According to the energy diagram (Fig. 8), the emission at 454 nm can be attributed to the $Tm^{3+1}D_2 \rightarrow {}^3F_4$ transition. Note that population of the $Tm^{3+1}D_2$ level via a fourth Yb^{3+} to Tm^{3+} energy transfer is very unlikely due to the large energy mismatch (around 3500 cm^{-1}) between the $Yb^{3+2}F_{5/2} - {}^2F_{7/2}$ and $Tm^{3+1}D_2 - {}^1G_4$ energy gaps.[30,32] The existence of the 454 nm emission band confirms that cross-relaxation processes 1) and 2) are relevant at high Tm^{3+} concentrations. At least two emission bands centered at around 365 and 454 nm arise from the $Tm^{3+1}D_2$ state. The decrease in $Tm^{3+3}H_4$ lifetimes with increasing Tm^{3+} concentration under 463 nm excitation [Fig. 7(a), Table S1 supplemental material[26]] is in good agreement with the existence of cross-relaxation mechanisms between Tm^{3+} ions via processes 1) and 2).

The lifetimes associated with the $Yb^{3+2}F_{5/2} \rightarrow {}^2F_{7/2}$ emission (1022 nm) decrease with increasing Tm^{3+} concentration [Fig. 7(a)]. This can be attributed to an increase in Yb^{3+} to Tm^{3+} energy transfer probabilities due to a decrease in the average Yb^{3+} to Tm^{3+} distance. Under 974 nm excitation, the lifetimes associated with the 479, 654, and 796 nm emissions from Y_2BaZnO_5: Yb^{3+} (10%), Tm^{3+} (y%) (y = 0.25, 0.5, 1, 2) samples also decrease with increasing dopant concentration, following the same trend as that of the $Yb^{3+2}F_{5/2}$ lifetimes [Fig. 7(a), Table S1 supplemental material[26]]. This suggests that the $Yb^{3+} - Tm^{3+}$ interaction dynamics govern the UC temporal behavior under 974 nm excitation, rather than the deexcitation lifetimes of the Tm^{3+} multiplets.[25]

C. Yb^{3+} concentration dependence of lifetimes

Under 463 nm excitation, the lifetimes associated with the 479 and 654 nm emissions (arising from $Tm^{3+1}G_4$) are almost invariant in the range of Yb^{3+} concentrations studied [Fig. 7(b), Table S1 supplemental material[26]]. This suggests that the intrinsic lifetime of $Tm^{3+1}G_4$ is almost unaffected by the Yb^{3+} concentration present in the samples. The very slight decrease in lifetimes with increasing Yb^{3+} concentration could be attributed to back-energy transfer between Tm^{3+} and Yb^{3+}, depopulating $Tm^{3+1}G_4$ at high Yb^{3+} concentrations. The existence of back-energy transfer mechanisms is further supported by the observation of a small intensity emission from Yb^{3+} centered around 1022 nm under selective Tm^{3+} excitation at 463 nm (Fig. S1, supplemental material[26]). Under 463 nm excitation, the lifetimes associated with the 796 nm emission (from $Tm^{3+3}H_4$) decrease with increasing Yb^{3+} concentration [Fig. 7(b), Table S1 supplemental material[26]] due to the back-energy transfer between Tm^{3+} and Yb^{3+}, depopulating $Tm^{3+3}H_4$ at high Yb^{3+} concentration.[35] The Yb^{3+} emission around 1022 nm is also observed under selective Tm^{3+} excitation at 790 nm (Fig. S2, supplemental material[26]), corroborating the presence of such back-energy transfers.

The lifetimes associated with the $Yb^{3+2}F_{5/2} \rightarrow {}^2F_{7/2}$ emission (1022 nm) decrease significantly with increasing Yb^{3+} concentration [Fig. 7(b)]. We have observed that excitation hopping between Yb^{3+} ions does not contribute significantly to the $Yb^{3+2}F_{5/2}$ lifetime, as no significant concentration dependence has been found with the Yb^{3+} concentration in singly doped samples. In addition, the lifetimes measured on Yb^{3+} singly doped samples were significantly higher than those of the Yb^{3+}, Tm^{3+} co-doped samples. The decrease in $Yb^{3+2}F_{5/2}$ lifetimes can therefore be attributed to an increase in Yb^{3+} to Tm^{3+} energy transfer rates. Under 974 nm excitation, the Yb^{3+} concentration dependence of the lifetimes associated with the 479, 654, and 796 nm emissions in Y_2BaZnO_5: Yb^{3+} (x%), Tm^{3+} (0.25%) (x = 0, 2, 6, 10) samples is significantly different from that observed under 463 nm excitation.

In particular, the $Tm^{3+1}G_4$ and $Tm^{3+3}H_4$ level lifetimes decrease markedly with increasing Yb^{3+} concentration, following the same trend as that of the $Yb^{3+2}F_{5/2}$ lifetimes. This supports the view that the dynamics of $Yb^{3+} - Tm^{3+}$ interactions play a dominant role in the observed upconversion emitting level lifetimes.

V. CONCLUSION

The upconversion properties of Y_2BaZnO_5: Yb^{3+}, Tm^{3+} oxide materials were investigated as a function of dopant concentration. Power dependence studies and lifetime measurements provide a model for the upconversion mechanisms involved in these materials. The strong near-infrared (796 nm) emission, which has an relatively high efficiency of up to $\sim 1.53\%$ (730-870 nm emission range), arises from the $Tm^{3+3}H_4$ level populated via two successive Yb^{3+} to Tm^{3+} energy transfer steps. This could find interesting applications in various fields of infrared technology.

The weaker blue (479 nm) and red (654 nm) emissions originate from $Tm^{3+1}G_4$ and involve three energy transfer steps. A maximum upconversion efficiency of $0.086 \pm 0.003\%$ (420-530 nm emission range) was obtained in Y_2BaZnO_5: Yb^{3+} (6%), Tm^{3+} (0.25%) at room temperature under ~ 2.5 W/cm^2 excitation. This opens up the possibility of combining the present Yb^{3+}, Tm^{3+} co-doped material with our Yb^{3+}, Er^{3+} (red plus green) phosphor[24] in order to produce white light. We shall explore this possibility in a future publication.

ACKNOWLEDGMENTS

This work was supported by the Saint-Gobain Recherche Company, France. I.H. acknowledges support by the Royal Academy of Engineering/EPSRC.

[1]F. Auzel, C. R. Acad. Sci. (Paris) **263B**, 819 (1966).
[2]F. Auzel, C. R. Acad. Sci. (Paris) **262**, 1016 (1966).
[3]V. Ovsyankin and P. P. Feofilov, JETP Lett. **4**, 317 (1966).
[4]J. J. Owen, A. K. Cheetham, and R. A. McFarlane, J. Opt. Soc. Am. B **15**, 684 (1998).
[5]B. R. Reddy, S. K. Nash-Stevenson, and P. Vankateswarlu, J. Opt. Soc. Am. B **11**, 923 (1994).
[6]Y. H. Wang and J. Ohwaki, Appl. Phys. Lett. **63**, 3268 (1993).
[7]S. Tanabe, S. Yoshii, K. Hirao, and N. Soga, Phys. Rev. B **45**, 4620 (1992).
[8]M. P. Hehlen, N. J. Cockroft, T. R. Gosnell, and A. J. Bruce, Phys. Rev. B **56**, 9302 (1997).
[9]I. R. Martín, V. D. Rodríguez, Y. Guyot, S. Guy, G. Boulon, and M. F. Joubert, J. Phys.: Condens. Matter. **12**, 1507 (2000).
[10]D. S. Funk and J. G. Eden, IEEE J. Sel. Top. Quantum Electron. **1**, 784 (1995).
[11]A. Patra, C. S. Friend, R. Kapoor, and P. N. Prasad, J. Phys. Chem. B **106**, 1909 (2002).
[12]J. A. Capobianco, F. Vetrone, J. C. Boyer, A. Speghini, and M. Bettinelli, Opt. Mater. **19**, 259 (2002).
[13]S. Tanabe, K. Suzuki, N. Soga, and T. Hanada, J. Opt. Soc. Am. B **11**, 933 (1994).
[14]D. C. Hanna, R. M. Percival, I. R. Perry, R. G. Smart, J. E. Townsend, and A. C. Tropper, Opt. Commun. **78**, 187 (1990).
[15]N. Rakov, G. S. Maciel, M. L. Sundheimer, S. L. D. Menezes, A. S. L. Gomes, Y. Messaddeq, F. C. Cassanjes, G. Poirier, and S. J. L. Ribeiro, J. Appl. Phys. **92**, 6337 (2002).
[16]I. R. Martín, J. Méndez-Ramos, V. D. Rodríguez, J. J. Romero, and J. García-Solé, Opt. Mater. **22**, 327 (2003).
[17]J. F. Suyver, J. Grimm, M. K. van Veen, D. Biner, K. W. Krämer, and H. U. Güdel, J. Lumin. **117**, 1 (2006).
[18]R. J. Thrash and L. J. Johnson, J. Opt. Soc. Am. B **11**, 881 (1994).
[19]Q. Y. Zhang, T. Li, Z. H. Jiang, X. H. Ji, and S. Buddhudu, Appl. Phys. Lett. **87**, 171911 (2005).
[20]T. Komukai, T. Yamamoto, T. Sugawa, and Y. Miyajima, IEEE J. Quantum. Electron. **31**, 1880 (1995).
[21]C. Michel and B. Raveau, J. Solid State Chem. **43**, 73 (1982).
[22]C. Michel and B. Raveau, J. Solid State Chem. **49**, 150 (1983).
[23]A. Birkel, A. A. Mikhailovsky, and A. K. Cheetham, Chem. Phys. Lett. **477**, 325 (2009).
[24]I. Etchart, A. Huignard, M. Bérard, M. N. Nordin, I. Hernández, R. J. Curry, W. P. Gillin, and A. K. Cheetham, J. Mater. Chem. **20**, 3989 (2010).
[25]I. Etchart, I. Hernández, A. Huignard, M. Bérard, W. P. Gillin, R. J. Curry, and A. K. Cheetham, J. Mater. Chem. **21**, 1397 (2011).
[26]See supplementary material at http://dx.doi.org/10.1063/1.3549634 for emission spectra in the infrared, and for information on upconversion efficiency and lifetime measurements.
[27]R. Buisson and J. C. Vial, J. Phys. Lett. **42**, L115 (1981).
[28]E. Nakazawa, in Phosphor Handbook, edited by S. Shionoya and W. M. Yen (CRC Press, Boca Raton, 1999), Chap. 2, p. 101.
[29]G. H. Dieke, *Spectra and Energy Levels of Rare Earth Ions in Crystals* (Interscience, New York, 1968).
[30]N. K. Giri, S. K. Singh, D. K. Rai, and S. B. Rai, Appl. Phys. B **99**, 271 (2010).
[31]R. Lisiecki, G. Dominiak-Dzik, T. Lukasiewicz, and W. Ryba-Romanowski, J. Mol. Struct. **704**, 323 (2004).
[32]X. B. Chen and Z. F. Song, J. Opt. Soc. Am. B **24**, 965 (2007).
[33]W. Guo, Y. Chen, Y. Lin, X. Gong, Z. Luo, and Y. Huang, J. Phys. D: Appl. Phys. **41**, 115409 (2008).
[34]Z. Xu, Y. Chen, Y. Lin, X. Gong, Z. Luo, and Y. Huang, J. Alloys Compd **481**, 411 (2009).
[35]F. Pandozzi, F. Vetrone, J. C. Boyer, R. Naccache, J. A. Capobianco, A. Speghini, and M. Bettinelli, J. Phys. Chem. B **109**, 17400 (2005).